Chitinase 3–like–1 and its receptors in Hermansky-Pudlak syndrome–associated lung disease

Yang Zhou,[1] Chuan Hua He,[1] Erica L. Herzog,[2] Xueyan Peng,[2] Chang-Min Lee,[1] Tung H. Nguyen,[1] Mridu Gulati,[2] Bernadette R. Gochuico,[3] William A. Gahl,[3] Martin L. Slade,[4] Chun Geun Lee,[1] and Jack A. Elias[1]

[1]Department of Molecular Microbiology and Immunology, Division of Medicine and Biologic Sciences, Brown University, Providence, Rhode Island, USA. [2]Section of Pulmonary, Critical Care and Sleep Medicine, Department of Internal Medicine, Yale University School of Medicine, New Haven, Connecticut, USA. [3]Medical Genetics Branch, National Human Genome Research Institute (NHGRI), NIH, Bethesda, Maryland, USA. [4]Section of Occupational Medicine, Department of Internal Medicine, Yale University School of Medicine, New Haven, Connecticut, USA.

Hermansky-Pudlak syndrome (HPS) comprises a group of inherited disorders caused by mutations that alter the function of lysosome-related organelles. Pulmonary fibrosis is the major cause of morbidity and mortality in patients with subtypes HPS-1 and HPS-4, which both result from defects in biogenesis of lysosome-related organelle complex 3 (BLOC-3). The prototypic chitinase-like protein chitinase 3–like–1 (CHI3L1) plays a protective role in the lung by ameliorating cell death and stimulating fibroproliferative repair. Here, we demonstrated that circulating CHI3L1 levels are higher in HPS patients with pulmonary fibrosis compared with those who remain fibrosis free, and that these levels associate with disease severity. Using murine HPS models, we also determined that these animals have a defect in the ability of CHI3L1 to inhibit epithelial apoptosis but exhibit exaggerated CHI3L1-driven fibroproliferation, which together promote HPS fibrosis. These divergent responses resulted from differences in the trafficking and effector functions of two CHI3L1 receptors. Specifically, the enhanced sensitivity to apoptosis was due to abnormal localization of IL-13Rα2 as a consequence of dysfunctional BLOC-3–dependent membrane trafficking. In contrast, the fibrosis was due to interactions between CHI3L1 and the receptor CRTH2, which trafficked normally in BLOC-3 mutant HPS. These data demonstrate that CHI3L1-dependent pathways exacerbate pulmonary fibrosis and suggest CHI3L1 as a potential biomarker for pulmonary fibrosis progression and severity in HPS.

Introduction

Hermansky-Pudlak syndrome (HPS) is a group of inherited autosomal recessive disorders that occur worldwide (1). Nine genetic subtypes (HPS1–9) have been described, with each mutation affecting the function of lysosome-related organelles (LROs). HPS-1 is particularly common in northwest Puerto Rico, where 1:1,800 people are affected, and the carrier frequency is 1 in 21 persons (1). The signs and symptoms of HPS are related to the dysfunction of a variety of LROs (2, 3). The dysfunction of melanosomes accounts for the oculocutaneous albinism and visual impairment found in all HPS patients (4). The dysfunction of platelet-dense granules accounts for the bleeding disorder that is often the presenting complaint of the disease (4, 5). Ceroid deposition also occurs in multiple organs, and inflammatory bowel disease has been reported in various subtypes of HPS (2, 6–8). More importantly, pulmonary fibrosis has been observed in HPS-1 and HPS-4 patients, whose genetic defects are in biogenesis of lysosome-related organelle complex 3 (BLOC-3), which includes HPS1 and HPS4 proteins; and, less commonly, in HPS-2 patients (3, 9–12). To date, pulmonary fibrosis has not been reported in patients with BLOC-2 defects (i.e., HPS-3, HPS-5, or HPS-6). Due to the untreatable and progressive nature of the pulmonary fibrosis of HPS, this complication is the leading cause of death (13). However, there is no way to predict which HPS-1 or HPS-4 patients are at risk for lung disease, or which patients will progress most rapidly. In addition, although it is known that murine genetic models of HPS-1 manifest exaggerated injury and fibroproliferative repair responses to fibrogenic agents such as bleomycin (14), the mechanism(s) by which LRO-related defects in trafficking lead to injury and fibrosis have not been adequately defined. Furthermore, no plausible explanation for why fibrosis develops in patients with BLOC-3 mutations and not in patients with BLOC-2 mutations has been put forth. Thus, the field would benefit greatly from insights that clarify the mechanisms by which LRO dysfunction leads to injury and fibroproliferative repair and studies that highlight the relationship(s) between these mechanisms and the occurrence and severity of lung disease in HPS.

The 18 glycosyl hydrolase (GH 18) gene family contains true chitinases (Cs) that degrade chitin polysaccharides and chitinase-like proteins (CLPs) that bind but do not degrade chitin (15). GH 18 genes are members of an ancient gene family that exists in species as diverse as plants, insects, and humans, and whose evolution during speciation is characterized by a particularly impressive increase in CLPs coinciding with the appearance of mammals (16, 17). Retention of GH 18 genes across species and evolutionary time has led to the belief that some of these moieties play essential roles in biology. Recent studies have confirmed this speculation (15, 18–21), particularly for the prototypic CLP, chitinase 3-like-1 (CHI3L1; also called YKL-40 in humans and BRP-39 in mice). CHI3L1 has been shown by our laboratory and others to play major roles in anti-pathogen, antigen-induced, and oxidant-induced

Authorship note: Yang Zhou and Chuan Hua He contributed equally to this work.
Conflict of interest: The authors have declared that no conflict of interest exists.
Submitted: October 31, 2014; **Accepted:** May 21, 2015.
Reference information: *J Clin Invest*. 2015;125(8):3178–3192. doi:10.1172/JCI79792.

inflammation, repair, and remodeling responses by regulating a variety of essential biologic processes, including oxidant injury, apoptosis, pyroptosis, inflammasome activation, Th1/Th2 inflammatory balance, M2 macrophage differentiation, TGF-β1 elaboration, dendritic cell accumulation and activation, and MAPK and AKT signaling (18, 20–25). The potential importance of CHI3L1-induced responses can also be seen in the large number of diseases characterized by inflammation and remodeling in which CHI3L1 excess has been documented (reviewed in refs. 15, 26). In many of these disorders, CHI3L1 is likely produced as a protective response based on its ability to simultaneously decrease epithelial cell apoptosis while stimulating fibroproliferative repair (27). Recent studies from our laboratory have defined IL-13Rα2 as the first receptor for any GH 18 moiety and have demonstrated that it mediates many of the effects of CHI3L1 (28). However, the regulation and roles of CHI3L1 and its receptors in HPS have not to our knowledge been addressed.

We hypothesized that CHI3L1 is dysregulated in HPS patients with BLOC-3 defects and plays an important role(s) in the pathogenesis of HPS lung disease. To test this, we measured the levels of CHI3L1 in plasma from patients with various types of HPS and assessed the relationships between these levels and the presence and severity of lung disease. We also used WT and *Hps1* mutant mice to characterize the roles of CHI3L1 and its receptors in the injury and fibroproliferative repair responses induced by intratracheal bleomycin. Our results demonstrate that levels of circulating CHI3L1 are increased in patients with HPS-1 and HPS-4 when compared with controls and non–BLOC-3 HPS patients and that, in the BLOC-3 patients, these levels correlate with the presence and severity of lung disease. CHI3L1 levels are increased in *Hps1* mutant mice at baseline and after bleomycin treatment, and null mutations of *Hps1* cause exaggerated bleomycin-induced epithelial cell apoptosis and fibrotic responses. These murine studies also demonstrate that CHI3L1 inhibits injury and stimulates repair in WT mice. In contrast, in *Hps1* mutant mice, the ability of CHI3L1 to stimulate fibroproliferation is preserved, but its ability to control epithelial apoptosis is markedly diminished. Last, we provide insights into the mechanisms that underlie these seemingly opposed responses by demonstrating that they are due to differences in the trafficking, localization, and function of two different CHI3L1 receptors. Specifically, the abnormal regulation of apoptosis is due to abnormal BLOC-3– and Rab32/38–dependent plasma membrane trafficking and localization of IL-13Rα2, and can be overcome with IL-13Rα2 overexpression. In contrast, the exaggerated collagen accumulation is mediated by CHI3L1 interaction with CRTH2, which traffics normally in *Hps1* mutant cells and tissues, and CRTH2 inhibition significantly diminishes this CHI3L1-induced fibrotic response.

Results

Levels of CHI3L1 are increased in the circulation of HPS-1 and HPS-4 patients. To determine whether CHI3L1 is dysregulated in HPS, we measured the levels of circulating CHI3L1 in patients older than 18 years of age with HPS and controls who had been assessed for the presence or absence of pulmonary fibrosis. One hundred forty-seven plasma samples from HPS patients were obtained. Of these, 129 had BLOC-3–related HPS (125 HPS-1 and 4 HPS-4) and 18 had BLOC-2–related HPS (12 HPS-3, 4 HPS-5, and 2 HPS-6). No other demographic information was available for the HPS subjects. Plasma from age-matched healthy controls was used as a control (n = 38). These assays revealed that CHI3L1 is elevated in the circulation of HPS-1 and HPS-4 (BLOC-3) patients compared with age-matched normal controls (Figure 1A). Moreover, the levels of CHI3L1 were elevated in the circulation of HPS-1 and HPS-4 patients compared with HPS-3, HPS-5, and HPS-6 (BLOC-2) patients (Figure 1A), though the values in these subtypes also mildly exceeded those of normal controls (Figure 1A). Interestingly, among the HPS-1 patients, the levels of CHI3L1 did not differ between individuals with the common Puerto Rican mutation (a 16-base-pair duplication in exon 15) and those with less common mutations (Supplemental Figure 1A). These studies demonstrate that the levels of CHI3L1 are elevated in the circulation of patients with BLOC-3–related HPS, who are more likely to develop pulmonary fibrosis, compared with normal controls and with BLOC-2–related HPS patients, who will not develop pulmonary fibrosis.

Levels of CHI3L1 are elevated in HPS-1 and HPS-4 patients with pulmonary fibrosis. Having found that HPS-1 and HPS-4 patients had elevated concentrations of circulating CHI3L1, we next stratified these patients into those with and those without documented lung disease. We found that HPS-1 and HPS-4 patients with lung disease had significantly elevated levels of circulating CHI3L1 compared with HPS-1 and HPS-4 patients without known lung disease (Figure 1B). These results demonstrate that circulating CHI3L1 is highest in those HPS patients with BLOC-3 mutations who have known pulmonary fibrosis. Immunohistochemistry on lung tissues from HPS-1 patients further revealed that airway epithelial cells and macrophages were the major source of CHI3L1 (Supplemental Figure 1B).

Levels of CHI3L1 correlate with disease severity. We next sought to determine whether circulating CHI3L1 was associated with clinically relevant parameters of disease severity. For this analysis we stratified HPS-1 and HPS-4 patients with pulmonary fibrosis into mild disease (defined as forced vital capacity [FVC] ≥80% predicted), mild-moderate disease (defined as FVC between 60% and 79% predicted), and severe disease (defined as FVC ≤59% predicted). We found that the levels of circulating CHI3L1 were similar in patients with mild and moderate disease (Figure 1C). In contrast, although there was some overlap, patients with severe disease had levels of CHI3L1 that were elevated compared with mild and moderate disease patients (Figure 1C). The levels of CHI3L1 followed a similar pattern when assessed using the diffusing capacity of lung for carbon monoxide (DLCO). These evaluations demonstrated that patients with severe disease had the highest levels of CHI3L1 (Figure 1D). In accordance with these findings, the levels of CHI3L1 displayed a modest but significant negative correlation with FVC (Figure 1E) and a negative correlation with DLCO (Figure 1F).

Levels of CHI3L1 are elevated in pale ear mice, a mouse model of HPS-1. The *pale ear* mouse, which has a null mutation of the *Hps1* gene ($Hps1^{ep}$), shares many aspects of the human disease phenotype (14, 29). To determine whether CHI3L1 is dysregulated in *pale ear* mice, we evaluated lung lysate *Chi3l1* mRNA and bronchoalveolar lavage (BAL) CHI3L1 protein in WT and *pale ear* mice at baseline and after bleomycin challenge. These assessments were

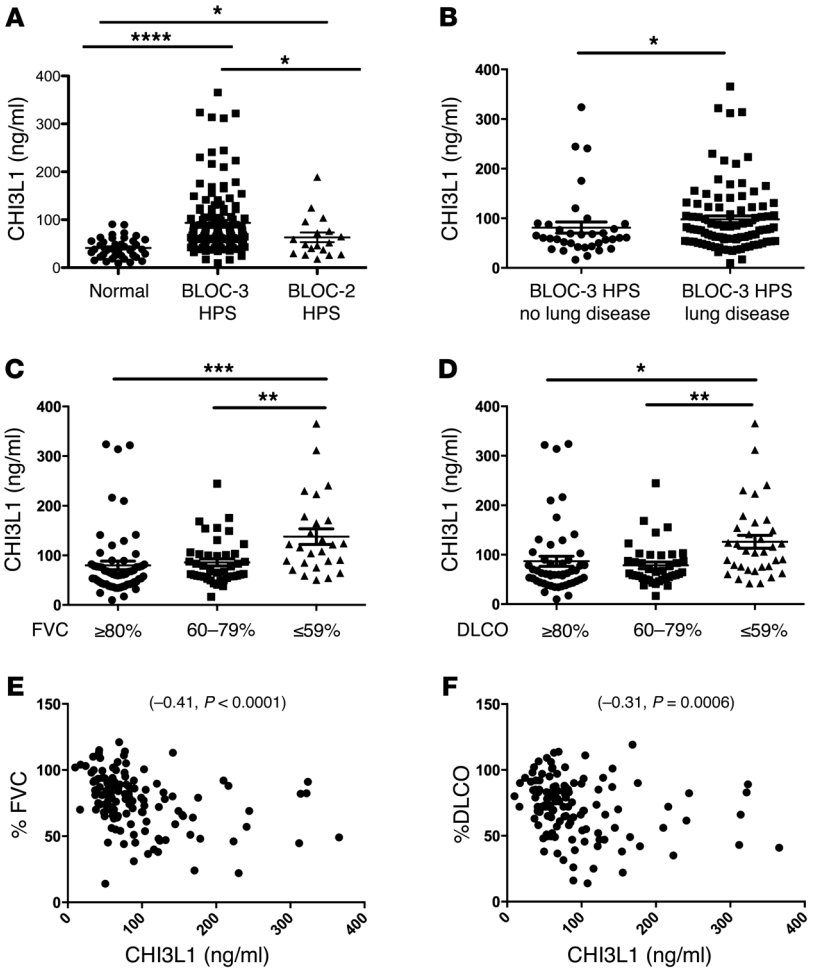

Figure 1. CHI3L1 levels are increased in HPS patients. (**A**) Plasma CHI3L1 is increased in HPS-1 (n = 125) and HPS-4 (n = 4) patients compared with age-matched normal controls (n = 38) and HPS-3, HPS-5, and HPS-6 patients (n = 18). (**B**) Plasma CHI3L1 is increased in HPS-1 and HPS-4 patients with lung disease (n = 94) compared with patients without lung disease (n = 35). The samples represent the two subsets of the BLOC-3 HPS samples shown in **A**. (**C**) Plasma CHI3L1 is higher in patients with severe disease according to FVC (n = 61 [FVC ≥80%], n = 42 [FVC 60%–79%], and n = 26 [FVC ≤59%]). (**D**) Plasma CHI3L1 is higher in patients with severe disease according to DLCO (n = 51 [DLCO ≥80%], n = 39 [DLCO 60%–79%], and n = 34 [DLCO ≤59%]). (**E**) Plasma CHI3L1 levels correlate with FVC (n = 129). (**F**) Plasma CHI3L1 levels correlate with DLCO (n = 129). Nonparametric data were assessed using Mann-Whitney U analysis (**A** and **B**) or Spearman correlations (**E** and **F**). Normally distributed data were compared using ANOVA with Bonferroni's post hoc test (**C** and **D**). $^*P \le 0.05$, $^{**}P \le 0.05$, $^{***}P \le 0.001$, $^{****}P \le 0.0001$.

undertaken during the injury and fibroproliferative repair phases of the bleomycin response. At baseline, the levels of CHI3L1 were elevated in the lungs of *pale ear* mice compared with WT controls (Figure 2, A and B). In WT mice, bleomycin administration caused early tissue injury that was associated with a significant decrease in tissue and BAL CHI3L1 (Figure 2, A and B). During the fibroproliferative phase (days 5–14), the levels of CHI3L1 returned to normal (Figure 2, A and B). Interestingly, the levels of tissue and BAL CHI3L1 in *pale ear* mice were increased on days 0, 10, and 14 and exceeded the baseline levels in WT mice at the later time points (Figure 2, A and B). At these time points immunohistochemistry demonstrated that epithelial cells and macrophages were the major sources of CHI3L1 in *pale ear* mice (Supplemental Figure 2 and data not shown). These studies demonstrate that the expression of CHI3L1 is increased at baseline and during bleomycin-induced injury and repair in *pale ear* mice.

Levels of epithelial apoptosis and tissue fibrosis are elevated in pale ear mice. Studies from our laboratory and others have demonstrated that injury is a prerequisite for the development of tissue fibrosis (30). Thus, studies were undertaken to evaluate both of these responses in WT mice and *pale ear* mice after bleomycin administration. Dose response evaluations demonstrated that differences between these mice were most readily appreciated with 1.25 U/kg of bleomycin (Supplemental Figure 3A). Studies using this dose demonstrated that, in WT mice, bleomycin caused an acute injury response characterized by inflammation (Supplemental Figure 3B) and alveolar type II epithelial cell apoptosis on day 7 that was followed by enhanced collagen accumulation and tissue fibrosis on days 7 and 14 (Figure 2, C and D, Supplemental Figure 3, C and D, and Supplemental Figure 4A). At baseline *pale ear* mice had a modest increase in epithelial TUNEL staining (Figure 2C and Supplemental Figure 4A). These alterations were associated with moderately enhanced caspase-3 activation (Supplemental Figure 4B). They did not, however, manifest noticeable increases in lung collagen content (Figure 2D). Importantly, the differences in TUNEL staining, caspase-3 activation, and collagen content were exaggerated in bleomycin-treated *pale ear* mice. Specifically, after bleomycin administration *pale ear* mice manifested exaggerated levels of epithelial apoptosis (Figure 2C and Supplemental Figure 4A), caspase 3 activation (Supplemental Figure 4B), and total BAL protein content (a parameter of lung injury) (Supplemental Figure 4C). In addition, as described in the literature (14), *pale ear* mice also exhibited enhanced fibrotic responses compared with WT controls 7 and 14 days after bleomycin administration (Figure 2D and Supplemental Figure 3C).

Endogenous CHI3L1 does not regulate apoptosis but does regulate fibroproliferative repair in pale ear mice. We next compared the bleomycin-induced epithelial injury (apoptosis) and fibroproliferative repair (collagen accumulation) responses in WT mice, *Chi3l1*-null mice, *pale ear* mice, and *pale ear Chi3l1* double mutants. When

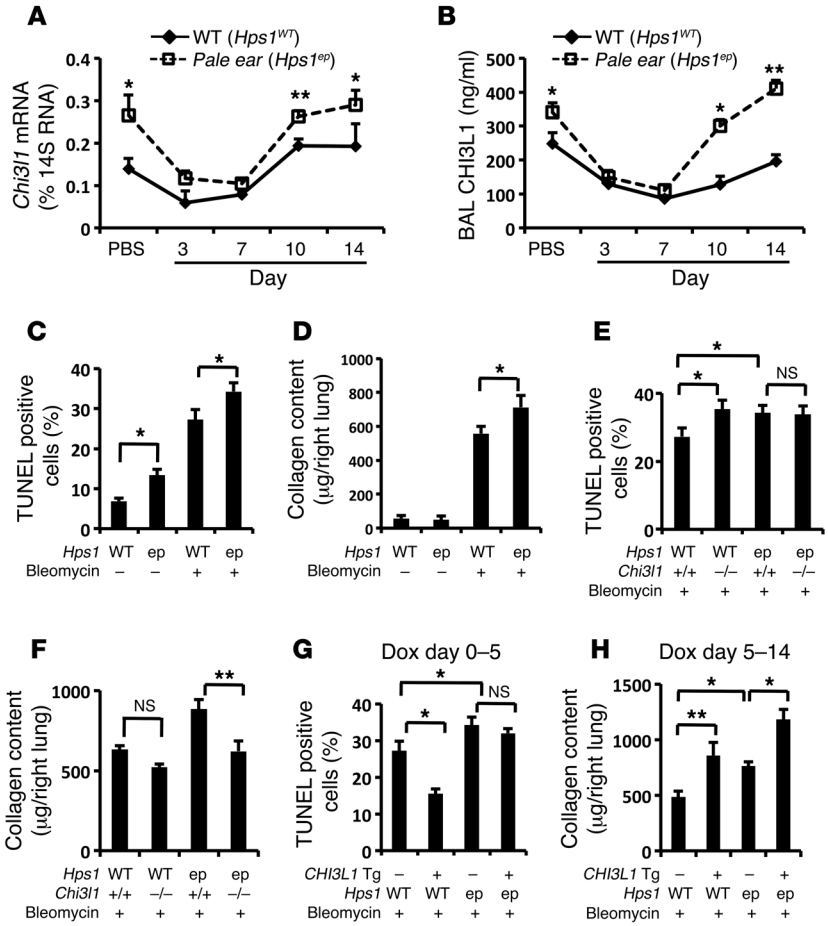

Figure 2. CHI3L1 levels are increased in the lungs of *pale ear* mice, and it does not regulate apoptosis but does regulate fibroproliferative repair in HPS. WT and *pale ear* (*Hps1*^{ep}) mice were employed. One group of WT and *pale ear* mice was sacrificed at day 3 (after administration of intratracheal PBS). Another cohort of WT and *pale ear* mice was given intratracheal bleomycin, and CHI3L1 was assessed 3, 7, 10, and 14 days later. (**A**) *Chi3l1* transcript was measured in whole-lung RNA extracts from WT and *pale ear* mice using qRT-PCR. (**B**) CHI3L1 protein levels in BAL fluid were quantified using ELISA. (**C**) TUNEL staining was performed on day 7, and TUNEL-positive type II epithelial cells were counted. (**D**) Total lung collagen was quantified using Sircol assay on day 14. (**E** and **F**) WT, *Chi3l1*$^{-/-}$, *pale ear*, and *Hps1*^{ep} *CHI3L1*$^{-/-}$ double mutant mice were subjected to intratracheal bleomycin administration. (**E**) All TUNEL-positive cells were counted on day 7. (**F**) Total lung collagen was quantified using Sircol assay on day 14. (**G** and **H**) WT, *CHI3L1* Tg, *pale ear*, and *Hps1*^{ep} *CHI3L1* Tg mice were subjected to intratracheal bleomycin administration. (**G**) *CHI3L1* Tg was turned on from day 0 to day 5. All TUNEL-positive cells were counted on day 7. (**H**) *CHI3L1* Tg was turned on from day 5 to day 14. Total lung collagen was quantified using Sircol assay on day 14. Values are mean ± SEM, with 6 mice in each group. Comparisons between groups were conducted by two-way ANOVA with Bonferroni's post hoc test. $^{**}P \le 0.01$, $^{*}P \le 0.05$. Dox, doxycycline.

compared with the WT controls, bleomycin-challenged *Chi3l1*-null mice and *pale ear* mice manifested exaggerated levels of apoptosis and BAL protein (Figure 2E and Supplemental Figure 5A). In contrast, the levels of collagen accumulation in *Chi3l1* mutant and *pale ear* mice were comparable to and exceeded, respectively, those of WT controls (Figure 2F). Importantly, the exaggerated bleomycin-induced epithelial cell death and lung injury response in *pale ear* mice was not altered by an absence of *Chi3l1* (Figure 2E and Supplemental Figure 5A). In contrast, the enhanced fibrotic response in *pale ear* mice was significantly diminished in the absence of *Chi3l1* (Figure 2F). In accordance with these later findings, the levels of mRNA encoding α1-procollagen and fibronectin and the levels of BAL TGF-β1 were significantly decreased in *pale ear Chi3l1* double mutant mice compared with *pale ear* mice (Supplemental Figure 5, B–D). These studies demonstrated that endogenous CHI3L1 regulates bleomycin-induced epithelial apoptosis and tissue fibrosis in WT mice but only regulates fibrosis in *pale ear* mice.

Transgenic CHI3L1 rescues the bleomycin-induced type II epithelial cell apoptosis in WT but not in pale ear mice. To further define the roles of CHI3L1 in the injury phase of bleomycin-induced responses, we used *CHI3L1* transgenic mice [Tg(*Cc10-CHI3L1*)], herein referred to as *CHI3L1* Tg mice) developed in our laboratory, in which CHI3L1 was selectively and inducibly targeted to the lung using the *Cc10* promoter (20). In these experiments we generated *CHI3L1* Tg mice on WT and *pale ear* genetic backgrounds, activated the *CHI3L1* Tg only during the tissue injury phase (days 0–5) after bleomycin administration, and characterized the levels of apoptosis using TUNEL evaluations 7 days after bleomycin administration. BAL *CHI3L1* transgene expression levels were similar in the WT and *pale ear* mice on day 7 (between 500 and 600 ng/ml) (Supplemental Figure 6A). As noted above, bleomycin increased the levels of apoptosis and BAL protein leak in WT mice and caused an exaggerated injury response in *pale ear* mice (Figure 2G and Supplemental Figure 6B). Interestingly, transgenic CHI3L1 markedly decreased the bleomycin-induced apoptosis and BAL protein leak in the WT mice (Figure 2G and Supplemental Figure 6B). Importantly, transgenic CHI3L1 did not rescue the apoptosis or BAL protein leak phenotype in *pale ear* mice (Figure 2G and Supplemental Figure 6B). This demonstrates that CHI3L1 has important antiapoptotic effects in bleomycin-treated WT mice and that this protective response is blunted in mice with null mutations of *Hps1*.

Transgenic CHI3L1 exaggerates bleomycin-induced fibroproliferative repair in WT and pale ear mice. We also used the *CHI3L1* Tg mice to further define the roles of CHI3L1 in bleomycin-induced fibrproliferative repair. We administered bleomycin to WT and *pale ear* mice and activated the *CHI3L1* transgene only during the fibroproliferative phase (days 5–14) of this response. This resulted in similar levels of BAL CHI3L1 (between 550 and 650 ng/ml) in the WT and *pale ear* mice (Supplemental Figure 6C). In these experiments, transgenic CHI3L1 significantly increased collagen accumulation in lungs from both WT and *pale ear* mice (Figure 2H and Supplemental Figure 6D). In accordance with these findings,

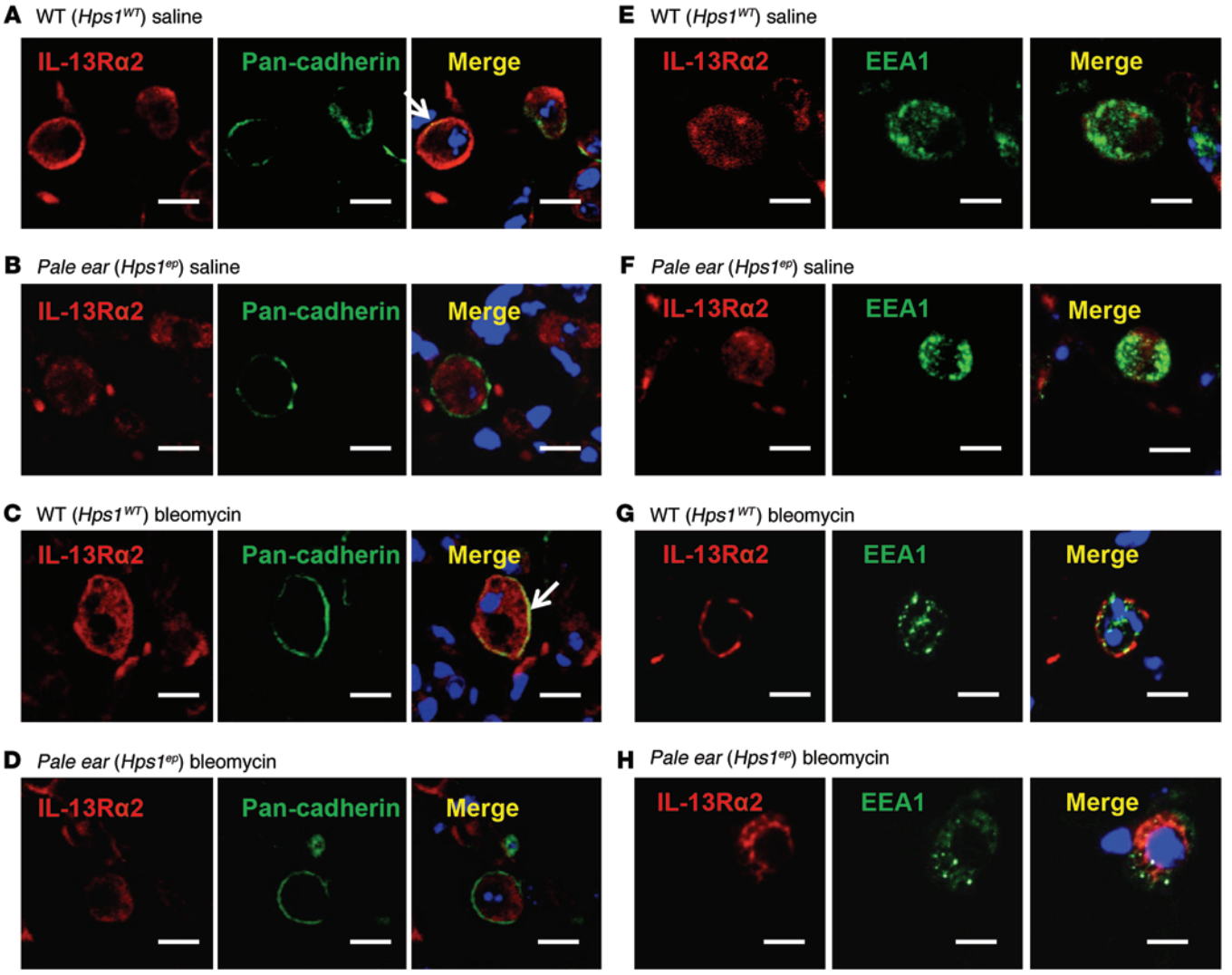

Figure 3. IL-13Rα2 membrane trafficking is impaired in *pale ear* mice. (**A**–**D**) WT and *pale ear* mice were treated with saline or bleomycin, and lungs were harvested on day 7. IL-13Rα2 was labeled with red fluorescence (Alexa Fluor 594). Pan-cadherin was labeled with green fluorescence (Alexa Fluor 488) to indicate plasma membrane. Localization of IL-13Rα2 on plasma membrane is indicated by arrows. Scale bars: 10 μm. (**E**–**H**) WT and *pale ear* mice were treated with saline or bleomycin, and lungs were harvested on day 7. IL-13Rα2 was labeled with red fluorescence (Alexa Fluor 594). EEA1 was labeled with green fluorescence (Alexa Fluor 488) to indicate endosomal compartment. Nuclei are stained with TO-PRO (Life Technologies) (blue). Each experiment was undertaken at least three times. Scale bars: 10 μm.

the transgenic expression of CHI3L1 also increased the levels of mRNA encoding α1-procollagen and fibronectin, and the levels of BAL TGF-β1, in WT mice and caused even more substantial increases in these parameters in *pale ear* mice (Supplemental Figure 6, E–G). These studies demonstrate that, when overexpressed only during the fibroproliferative repair phase of the bleomycin-induced response, CHI3L1 stimulates fibrosis and matrix gene expression in WT mice and mice with null mutations of *Hps1*.

IL-13Rα2 membrane localization is impaired in pale ear mice. The studies noted above highlight a defect in the ability of CHI3L1 to control epithelial cell apoptosis in *pale ear* mice. Recent studies from our laboratory have described the first receptor for CHI3L1 or any GH 18 moiety. These studies demonstrated that CHI3L1 binds to, signals, and controls apoptosis via IL-13Rα2 (28). Hence, we sought to determine whether IL-13Rα2 localization is altered in the setting of BLOC-3 mutations. In these experiments lungs were obtained from WT and *pale ear* mice that had been treated with bleomycin or from controls, and IL-13Rα2 immunofluorescence staining was performed using pan-cadherin or early endosome antigen 1 (EEA1) markers to highlight the plasma membrane and intracellular/endosomal compartments, respectively. In keeping with the literature, in WT mice at baseline, IL-13Rα2 was expressed both intracellularly and on the cell membrane (Figure 3, A and E). In contrast, in *pale ear* mouse lung, IL-13Rα2 was expressed at lower levels, and the cytoplasmic pool was readily noted, but the membrane pool could not be detected (Figure 3, B and F). Importantly, bleomycin treatment caused substantial IL-13Rα2 membrane translocation in the WT lungs, as indicated by its colocalization with cadherin (Figure 3, C and G). In contrast, IL-13Rα2 remained in the intracellular space in bleomycin-treated *pale ear* mouse lungs, demonstrating that its localization to plasma membrane was impaired (Figure 3, D and H). Western blot analysis confirmed these observations. In

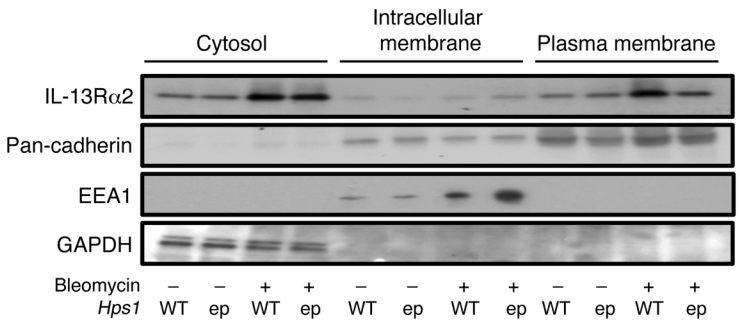

Figure 4. IL-13Rα2 membrane trafficking is impaired in *pale ear* mice. Total protein was extracted from the cytosolic fraction, intracellular membrane fraction, or plasma membrane fraction of WT and *pale ear* mouse lung. Western blot analysis was performed to detect IL-13Rα2. Pan-cadherin, EEA1, and GAPDH were used as specificity and loading controls. Each experiment was undertaken at least three times.

WT lung lysates, IL-13Rα2 could be detected in the cytosol, intracellular membrane fraction, and plasma membrane fraction, while membrane localization of IL-13Rα2 was markedly diminished in *pale ear* mouse lungs (Figure 4).

IL-13Rα2 localization and trafficking is different in cells from WT and pale ear mice. To further understand the role(s) of IL-13Rα2 in the defective CHI3L1 regulation of epithelial apoptosis in *pale ear* mice, we isolated alveolar type II cells from lungs of WT and *pale ear* mice and assessed the localization and trafficking of IL-13Rα2 in these cells. Consistent with our in vivo findings, IL-13Rα2 membrane translocation was readily detected in cells from WT mice following bleomycin stimulation (Figure 5, A and B). In contrast, IL-13Rα2 remained in the intracellular fraction in bleomycin-treated *pale ear* cells (Figure 5, A and B).

In order to track cellular IL-13Rα2 protein movements, we employed a green fluorescent protein label. In these experiments an IL-13Rα2–GFP fusion protein expression plasmid was constructed and expressed in primary WT and primary *pale ear* type II alveolar epithelial cells. Live cell confocal imaging was then employed to localize the tagged IL-13Rα2 over time. These studies demonstrated that bleomycin stimulated IL-13Rα2–GFP fusion protein membrane translocation in WT cells (Figure 5C). In contrast, under identical circumstances, substantial membrane translocation was not detected, and the majority of the IL-13Rα2 remained in the intracellular compartment in *pale ear* cells (Figure 5D). These results demonstrate that IL-13Rα2 exists in an intracellular pool and can be mobilized to the plasma membrane after stimulation with agents such as bleomycin. In addition, they demonstrate that IL-13Rα2 trafficking to the plasma membrane is impaired in *pale ear* cells and thus is dependent on a pathway that involves the BLOC-3 complex.

The levels of IL-13Rα2 expression are similar at baseline and modestly decreased after bleomycin treatment in pale ear mice. The studies noted above demonstrate that IL-13Rα2 accumulation and localization are different in *pale ear* and WT mice. To further understand these differences, we evaluated the levels of mRNA encoding IL-13Rα2 in these mice at baseline and after bleomycin treatment. As also noted above, at baseline, *pale ear* mice had elevated levels of apoptosis and BAL CHI3L1. Despite these changes, at baseline, *pale ear* and WT mice had similar levels of mRNA encoding IL-13Rα2 (Supplemental Figure 7A). This demonstrates that differences in *Il13ra2* gene expression did not make a major contribution to the differences between WT and *pale ear* mice in the absence of bleomycin treatment. In contrast, the levels of mRNA encoding IL-13Rα2 were significantly increased in WT mice 7 to 14 days after bleomycin administration, and this response was modestly blunted in *pale ear* mice (Supplemental Figure 7A). Western blot analysis using whole lung lysates confirmed these findings (Supplemental Figure 7B). The findings demonstrate that differences in *Il13ra2* gene expression might also contribute in a modest manner to the IL-13Rα2 abnormalities that are seen in *pale ear* mice.

IL-13Rα2 rescues the antiapoptotic effects of CHI3L1 in primary type II epithelial cells from pale ear mice. Studies were next undertaken to define the functional consequences of the IL-13Rα2 abnormalities in *pale ear* mice. In these experiments we characterized the ability of CHI3L1 to inhibit the basal and bleomycin-induced apoptosis responses in alveolar type II epithelial cells from WT and *pale ear* mice. The cells from WT mice manifested a low level of basal apoptosis, which was markedly increased by bleomycin treatment (Figure 6A). The basal and bleomycin-induced cell death responses were exaggerated in cells from *pale ear* mice (Figure 6A). Recombinant CHI3L1 was a powerful inhibitor of bleomycin-induced apoptosis in cells from WT mice (Figure 6A). In contrast, it did not decrease the apoptosis in similarly treated cells from *pale ear* mice (Figure 6A). Transfection of cells from *pale ear* mice with high concentrations of a construct that expressed IL-13Rα2 allowed a membrane pool of IL-13Rα2 to be detected (Supplemental Figure 8). This treatment decreased the levels of basal apoptosis in cells from *pale ear* mice (Figure 6B). It also rescued the antiapoptotic effects of rCHI3L1 after bleomycin treatment (Figure 6B). In accordance with these findings, *Il13ra2*-null mutant mice had similarly increased basal levels of apoptosis (Supplemental Figure 9). These studies demonstrate that the abnormalities in IL-13Rα2 in *pale ear* mice play a critical role in the pathogenesis of the exaggerated apoptosis in these animals. They also demonstrate that an intervention that restores the membrane localization and expression of IL-13Rα2 rescues the anitapoptotic effects of CHI3L1 in unstimulated and bleomycin-treated *pale ear* epithelial cells.

The BLOC-3/Rab32/38 axis plays an important role in the antiapoptotic effects of IL-13Rα2. BLOC-3 is a guanine nucleotide exchange factor for the Rab small GTPase family member Rab32/38 (31). As a result, HPS1 and HPS4 are required for the normal trafficking and activation of Rab32/38. The studies noted above highlight a critical role of BLOC-3 in IL-13Rα2 membrane trafficking and its antiapoptotic response. To further understand this trafficking pathway, we treated type II epithelial A549 cells with siRNA that specifically silenced *HPS1*, *HPS4*, *RAB32*, or *RAB38* (Supplemental Figure 10, A–D). Bleomycin-induced IL-13Rα2 membrane accumulation was markedly diminished when the expression

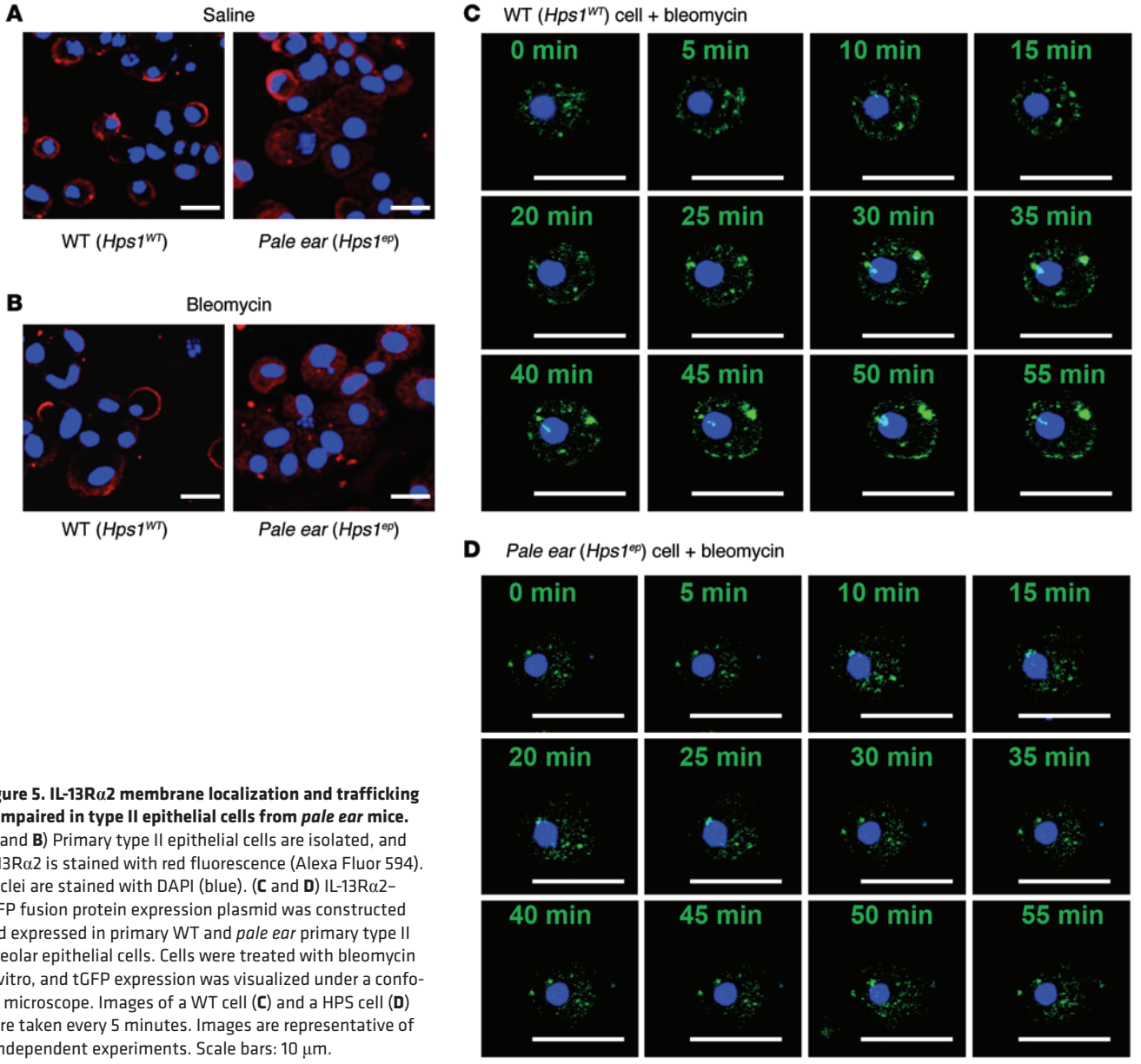

Figure 5. IL-13Rα2 membrane localization and trafficking is impaired in type II epithelial cells from *pale ear* mice. (**A** and **B**) Primary type II epithelial cells are isolated, and IL-13Rα2 is stained with red fluorescence (Alexa Fluor 594). Nuclei are stained with DAPI (blue). (**C** and **D**) IL-13Rα2–tGFP fusion protein expression plasmid was constructed and expressed in primary WT and *pale ear* primary type II alveolar epithelial cells. Cells were treated with bleomycin in vitro, and tGFP expression was visualized under a confocal microscope. Images of a WT cell (**C**) and a HPS cell (**D**) were taken every 5 minutes. Images are representative of 3 independent experiments. Scale bars: 10 μm.

of any of these moieties was diminished (Figure 6C), while the accumulation was not altered when *HPS3* or *RAB4A* was knocked down (Supplemental Figure 10E). In accordance with the findings noted above, bleomycin-induced apoptotic responses were exaggerated when the expression of HPS1, HPS4, Rab32, and/or Rab38 was diminished (Figure 6D), and IL-13Rα2 transfection could rescue this exaggerated apoptotic response (Figure 6E). These studies demonstrate that BLOC-3 and its target Rab32/38 are required for IL-13Rα2 membrane localization and its antiapoptotic effects.

CHI3L1 promotes fibroproliferation via CRTH2. The above studies demonstrate that CHI3L1 is induced and plays an antiapoptotic role during the injury phase of bleomycin administration. They also demonstrate that this cytoprotective effect is mediated via IL-13Rα2 and that, in *pale ear* mice, the ability of CHI3L1 to exert its antiapoptotic effects is diminished due to the abnormal localization of IL-13Rα2. In contrast, the fibrogenic effects of CHI3L1 were intact in WT and *pale ear* mice and did not utilize IL-13Rα2 in either setting. This suggested that CHI3L1 might mediate its fibroproliferative effects via a different receptor. To address this possibility, yeast two-hybrid evaluations were undertaken to define the binding partners of CHI3L1. This approach was the first to define IL-13Rα2 as a receptor for CHI3L1 (28). In addition to IL-13Rα2, one of the most intriguing positive clones encoded the prostaglandin D2 receptor CRTH2 (Supplemental Figure 11). The ability of CHI3L1 and CRTH2 to interact with one another was then assessed using co-immunoprecipitation (Co-IP) evaluations. These studies demonstrated that the two moieties physically bind one another, because the immunoprecipitation of one always brought down the other (Figure 7A). Immunoprecipitation with antibodies against unrelated controls such as IgG or galectin-3 did not yield similar results (Figure 7A and data not shown). Fluorescence-activated cell sorting (FACS) evaluations of non-permeabilized cells also demonstrated that CHI3L1 and CRTH2 are both expressed on the surface of the cell (Figure 7B). The role(s) of CRTH2 in imple-

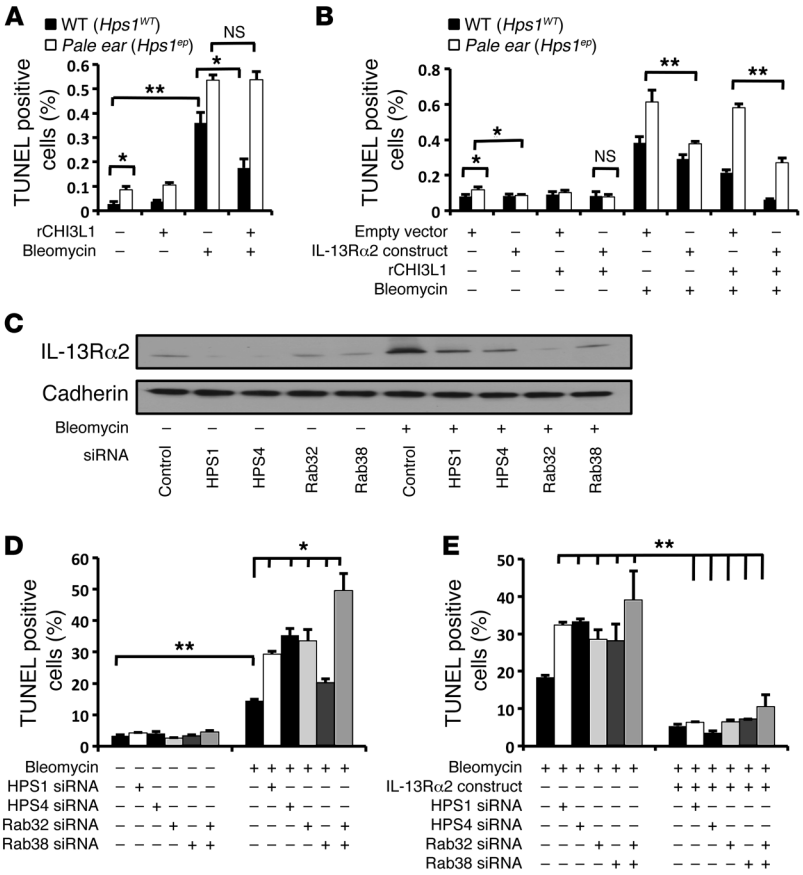

Figure 6. The BLOC-3/Rab32/38 axis plays an important role in the antiapoptotic effects of IL-13Rα2. Primary type II alveolar epithelial cells were extracted from WT and *pale ear* mice, pretreated with recombinant CHI3L1; transfected with empty vector or an IL-13Rα2 construct; and treated with bleomycin in vitro. (**A** and **B**) TUNEL staining was performed, and TUNEL-positive cells were counted. (**C**–**E**) A549 cells were treated with HPS1, HPS4, Rab32, and/or Rab38 siRNA, transfected with empty vector or IL-13Rα2 construct, and treated with bleomycin in vitro. (**C**) Total protein was extracted from the plasma membrane fraction, and Western blot analysis was performed to detect IL-13Rα2. Pan-cadherin was used as specificity and loading control. (**D** and **E**) TUNEL staining was performed, and TUNEL-positive cells were counted. Values are mean ± SEM, with three experiments. Comparisons between groups were conducted by two-way ANOVA with Bonferroni's post hoc test. $^*P \le 0.05$, $^{**}P \le 0.01$.

menting the fibroproliferative effects of bleomycin in WT, *pale ear*, and *CHI3L1* Tg mice were then evaluated. In these experiments, inhibition of CRTH2 decreased the levels of bleomycin-induced collagen accumulation in WT and *pale ear* mice (Figure 7C). In addition, the exaggerated fibrosis that was caused by activation of the *CHI3L1* transgene activation during fibroproliferative repair was also abrogated by CRTH2 inhibition (Figure 7D). Because M2 macrophages play an important role in fibrogenesis and studies from our laboratory have demonstrated that CHI3L1 is a powerful stimulator of M2 macrophage differentiation (27), studies were undertaken to determine whether CRTH2 played an important role in this response. As shown in Figure 7, E–G, CRTH2 plays an essential role in CHI3L1-induced M2 macrophage differentiation in vivo and in vitro. In accordance with these findings, the localization of CRTH2 was similar in lungs from WT and *pale ear* mice following bleomycin treatment (Figure 8, A and B). Furthermore, the levels of mRNA encoding CRTH2 (Supplemental Figure 12A) and the levels of CRTH2 protein in whole lung lysates (Supplemental Figure 12B) were similar at baseline and after bleomycin challenge in WT and *pale ear* mice. These studies demonstrate that the membrane localization of CRTH2 is similar in WT and *Hps1* mutant cells and tissues, and that CRTH2 plays a critical role in CHI3L1-induced fibroproliferative responses.

IL-13Rα2 membrane expression is decreased in HPS lung tissues. The studies noted above demonstrate that the trafficking of IL-13Rα2 to the cell membrane is decreased in bleomycin-treated lungs from *pale ear* versus WT mice. Studies were next undertaken to see whether similar results would be seen in lung tissues from HPS patients. In these experiments we compared the expression of IL-13Rα2 in tissues from normal individuals, HPS patients, and patients with idiopathic pulmonary fibrosis (IPF), who have fibrosis but do not have a HPS1 defect. As shown in Figure 8C, these studies highlight a modest IL-13Rα2 signal in lungs from normal individuals, most of which was intracellular. In keeping with the literature (32, 33), an enhanced IL-13Rα2 signal, some of which was localized to cell membranes, was seen in the samples from the IPF patients (Figure 8C). In contrast, in HPS lungs IL-13Rα2 was expressed at lower levels, and the cytoplasmic pool was readily noted but the membrane pool could not be detected (Figure 8C). These findings are consistent with our findings in mice demonstrating that IL-13Rα2 trafficking to the plasma membrane is impaired in HPS lung tissues.

Discussion

HPS-related pulmonary fibrosis develops in the fourth or fifth decade of life and is the leading cause of death in HPS-1 and HPS-4 patients (3, 9, 10, 13). Despite considerable effort to understand this disorder, the mechanisms that drive the lung injury and the progressive fibrotic response in HPS patients are not well defined, and no therapeutics successfully intervene in these responses. Our studies demonstrate that the levels of CHI3L1 are elevated in the circulation of BLOC-3 HPS patients (who are more likely to develop pulmonary fibrosis) compared with BLOC-2 HPS patients and controls and that, in BLOC-3 patients, the levels correlate with physiologic parameters of disease severity. Our results also demonstrate that CHI3L1 plays an important role

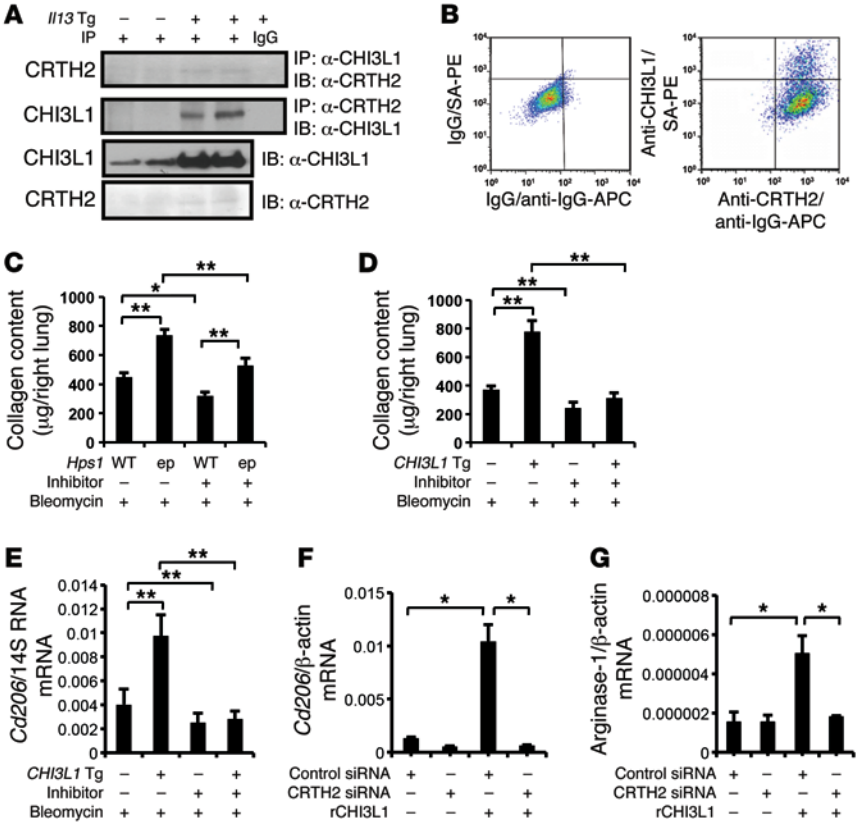

Figure 7. CHI3L1 binds to and promotes fibrosis development through CRTH2. (**A**) CHI3L1 and CRTH2 Co-IP. Immunoprecipitation (IP) of CHI3L1 or CRTH2 was undertaken, and the precipitate was then evaluated by Western immunoblot (IB) analysis as noted. Lung lysates from WT [*Il13* Tg (–)] and *Il13* Tg (+) mice were employed. (**B**) Colocalization of CHI3L1 and CRTH2. THP-1 cells were incubated in the presence or absence of anti-CHI3L1–biotin antibody or anti-CRTH2 IgG antibody without permeabilization. The cells were then washed and stained with streptavidin-PE (SA-PE) and anti-IgG–APC and subjected to flow cytometric analysis. Each experiment was undertaken at least three times.(**C**–**E**) WT, *pale ear*, and *CHI3L1* Tg mice were subjected to intratracheal bleomycin administration. Mice were treated with CRTH2 inhibitor or its vehicle control. (**C** and **D**) Total lung collagen was quantified using Sircol assay on day 14. (**E**) mRNA levels of *Cd206* were evaluated by qRT-PCR. The noted values are the mean ± SEM of evaluations of 6 mice in each group. (**F** and **G**) Mouse peritoneal macrophages were transfected with control or CRTH2 siRNA and treated with recombinant CHI3L1 (500 ng/ml) for 24 hours. mRNA levels of (**F**) *Cd206* and (**G**) arginase-1 were evaluated by qRT-PCR. The noted values are the mean ± SEM of 3 independent experiments. Comparisons between groups were conducted by 2-way ANOVA with Bonferroni's post hoc test. $^*P \le 0.05$, $^{**}P \le 0.01$.

in the pathogenesis of HPS pulmonary fibrosis. Specifically, in bleomycin-treated normal mice, CHI3L1 decreased epithelial injury while stimulating fibroproliferative repair. In contrast, in the *pale ear* mouse model of HPS-1, the ability of CHI3L1 to inhibit epithelial apoptosis was markedly blunted, while the fibroproliferative effects of CHI3L1 were augmented. This demonstrates that a defect in the CHI3L1 axis is a major contributor to the exaggerated sensitivity of HPS epithelium to injury-inducing and apoptotic stimuli (14, 34). We also provide insights into the mechanisms that underlie the defect in CHI3L1 inhibition of epithelial apoptosis and the augmented fibroproliferative repair in HPS. These studies demonstrate that IL-13Rα2, the receptor that CHI3L1 uses to mediate its antiapoptotic effect (28), does not localize properly to the cell membrane in *pale ear Hps1*-null cells and tissues. They also demonstrate that overexpression of IL-13Rα2 rescues this antiapoptotic effect. Simultaneously, they demonstrate that CHI3L1 also binds to CRTH2, that CRTH2 localizes normally in cells and tissues from *pale ear* mice, and that CHI3L1 utilizes CRTH2 to optimally promote tissue fibrotic responses. When viewed in combination, the studies demonstrate that defective CHI3L1 inhibition of epithelial apoptosis and exaggerated CHI3L1-CRTH2–driven fibroproliferation play important roles in the enhanced epithelial injury and fibrosis of HPS. They also show that these effects are due to differential receptor localization, trafficking, and function. Specifically, IL-13Rα2 traffics to and accumulates in the plasma membrane via a BLOC-3–dependent mechanism, and a defect in the trafficking of this receptor is an important event in the exaggerated epithelial apoptosis in BLOC-3 HPS patients. In contrast, CRTH2 traffics normally in BLOC-3–defective cells and tissues, allowing the elevated levels of CHI3L1 to engender exaggerated fibroproliferative repair.

The fibrotic response in BLOC-3 HPS patients resembles that of IPF (3, 10, 35). Studies from our laboratory and others have demonstrated that injury and apoptosis are prerequisites for the development of fibrosis and tissue remodeling (30). However, only scant data exist regarding the simultaneous regulation of all phases of fibrogenesis in this or other fibrotic diseases. We are particularly lacking in our understanding of the responses that control epithelial apoptosis in the setting of oxidant and other injuries. Therefore, the discovery of a protein with the ability to exert compartment-specific effects upon different components of the fibrotic response is exciting. Our studies suggest that CHI3L1 is just such a moiety, with distinct roles in injury and repair. Specifically, in these and other studies in WT mice, CHI3L1 has protective effects that can be mediated by its ability to decrease epithelial apoptosis, inhibit inflammation, and decrease oxidant injury (36). CHI3L1 can also drive fibroproliferative repair by augmenting alternative macrophage activation, fibroblast proliferation, and extracellular matrix gene expression during the repair response. As noted above and in studies from other groups, HPS mouse models do not spontaneously develop fibrosis (37). However, they consistently manifest exaggerated sensitivity to fibrogenic, injurious, and apoptotic stimuli, and these exaggerated injury responses are believed to lead to the pulmonary fibrosis that follows (14, 29, 34, 37–42). Our studies add to this body of data by demonstrating, for the first time to our knowledge, that the CHI3L1 axis plays an essential role in the regulation of epithelial apoptosis and that this response is blunted in *pale ear* mice. Hence, interventions that

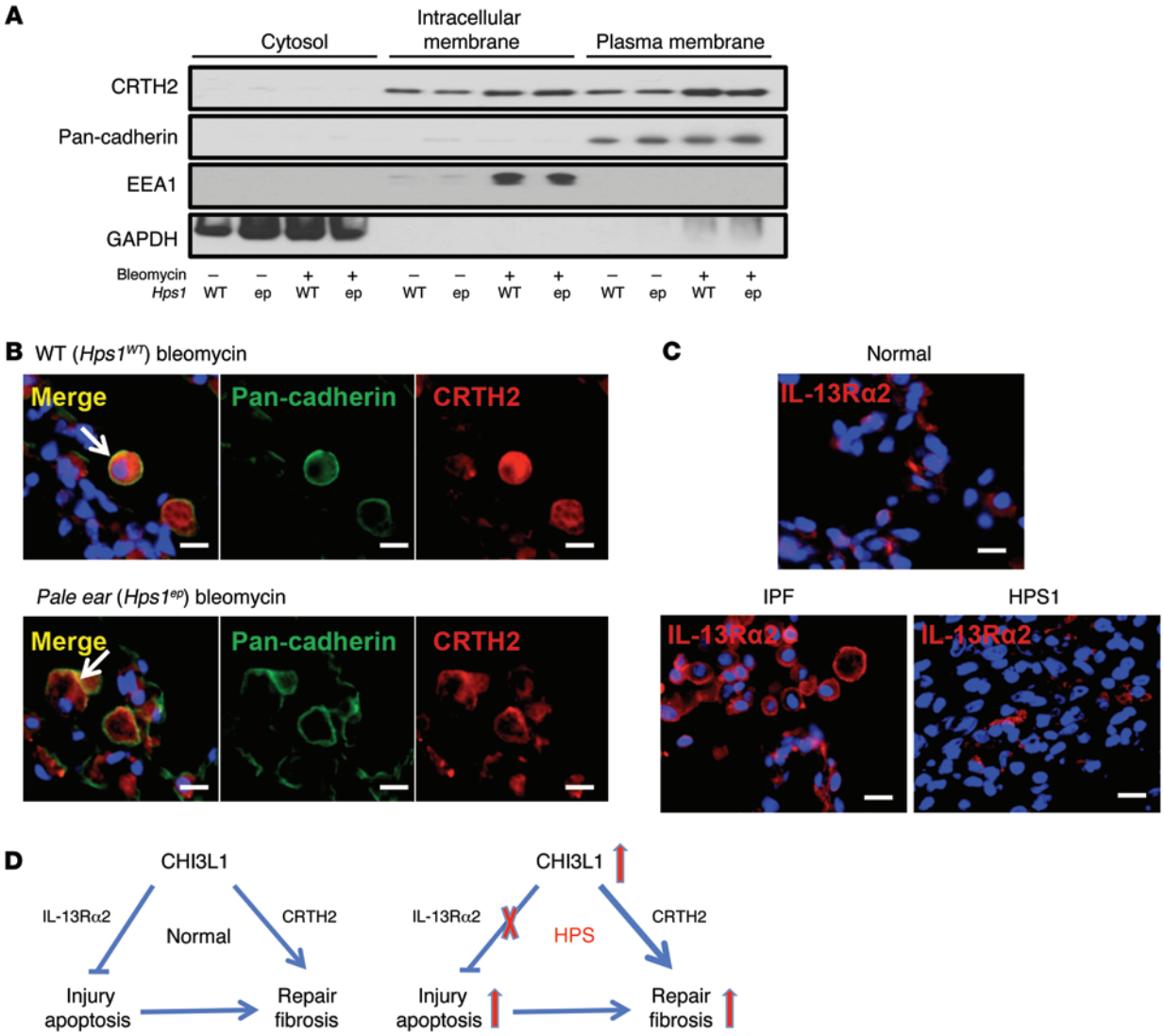

Figure 8. CRTH2 and IL-13Rα2 in HPS. (**A**) Total protein was extracted from bleomycin- or saline-treated WT and *pale ear* mouse lungs and separated into cytosolic, intracellular membrane, and plasma membrane fractions. Western blot analysis was performed to detect CRTH2. Pan-cadherin and GAPDH were used as specificity and loading controls. (**B**) Lungs from WT and *pale ear* mice were treated with bleomycin, CRTH2 was labeled with red fluorescence (Alexa Fluor 594), and pan-cadherin was labeled with green fluorescence (Alexa Fluor 488) to indicate plasma membrane. Localization of CRTH2 on plasma membrane is indicated by arrows. (**C**) Lung biopsies from normal, IPF, and HPS-1 patients were subject to immunofluorescence staining of IL-13Rα2. Nuclei are stained with DAPI (blue). Scale bars: 10 μm. Each experiment was undertaken at least three times. (**D**) A schematic diagram of CHI3L1-mediated injury and repair responses in normal and HPS individuals.

augment CHI3L1 can be therapeutically useful in controlling the injury phase of a variety of pulmonary disorders. However, this would not be as useful in patients with HPS-1 and HPS-4, where IL-13Rα2 trafficking is also altered (see below).

IL-13Rα2 was described as a high-affinity receptor for IL-13 that is distinct from the IL-13Rα1–IL-4Rα receptor dimer that IL-13 shares with IL-4 (43, 44). It was initially believed to be a decoy receptor (45). However, other studies demonstrated that IL-13 signals and regulates a variety of cellular and tissue responses via IL-13Rα2 (44, 46–52). Recent studies from our laboratory identified the first receptor for any GH 18 moiety by demonstrating that IL-13Rα2 binds to and is activated by CHI3L1 (28). These studies also showed that CHI3L1 mediates its antiapoptotic effects via this ligand-receptor interaction (28). Importantly, the majority of IL-13Rα2 exists in an intracellular cytoplasmic pool and traffics to the plasma membrane after appropriate cellular activation (53, 54). However, the mechanism(s) of IL-13Rα2 mobilization to the plasma membrane have not been defined. Our current studies demonstrate that IL-13Rα2 trafficking to the cell surface is mediated by a BLOC-3 complex–dependent pathway. In fact, insufficient IL-13Rα2 membrane localization is responsible for the enhanced apoptotic response in *pale ear* mice, and overexpression of IL-13Rα2 rescues the antiapoptotic effects of CHI3L1 in *pale ear* cells. These studies define, for the first time to our knowledge, the important role that abnormalities in IL-13Rα2 trafficking play in HPS. Studies by others have demonstrated that IL-13Rα2 is a critical downregulator of IL-13–mediated tissue fibrotic responses (55, 56). Additional investigation will be required to determine

whether these protective effects of IL-13Rα2 are mediated by CHI3L1 or if IL-13 signaling contributes to fibrogenesis in HPS. Nevertheless, our studies suggest that interventions that increase IL-13Rα2 membrane localization could be beneficial in the treatment of BLOC-3 HPS patients.

The genes mutated in HPS encode subunits of the BLOCs. Until recently, the molecular functions of the HPS1-HPS4 complex, BLOC-3, remained mysterious. We now know that BLOC-3 is a Rab32 and Rab38 guanine nucleotide exchange factor (GEF) and is required for melanosome cargo delivery and pigmentation (31), melanosome biogenesis (12, 31), and the trafficking of melanin-producing enzymes in melanocytes (31, 57). In the present studies we demonstrate, for the first time to our knowledge, that Rab32/38 also play critical roles in IL-13Rα2 trafficking and that loss of BLOC-3–mediated Rab32/38 activity can explain the type II lung epithelial cell dysfunction and apoptosis seen in *pale ear* mice. These studies allow for the interesting speculation that interventions that augment Rab32/38 can improve IL-13Rα2 trafficking and prove therapeutically useful in BLOC-3 HPS patients.

Recent studies from our laboratories have also demonstrated that galectin-3, a β-galactoside–binding lectin, is also dysregulated in HPS (58, 59). These studies demonstrated that the levels of galectin-3 are increased in the BAL and lungs of HPS patients. They also demonstrated that its accumulation was decreased in plasma membranes of fibroblasts from HPS patients. These findings suggest that galectin-3, like CHI3L1, also traffics abnormally in HPS. When viewed in combination, these observations allow for the possibility that the abnormal trafficking of moieties such as the 14 mammalian galectins and receptors of 18 glycosyl hydrolases may be a general feature of HPS. The appreciation that these moieties have far reaching effects on essential biologic processes, including cell adhesion activation growth and differentiation, apoptosis, and tissue repair, also allow for the interesting possibility that these trafficking abnormalities play essential roles in the pathogenesis of HPS. Additional investigation will be needed to assess the validity of these speculations. It will also be important to determine whether these moieties interact with one another and if BLOC-3–mediated Rab32/38 activity is also responsible for galectin-3 trafficking to the membrane.

CHI3L1 is produced by a wide variety of cells, including macrophages, epithelial cells, and chondrocytes and is markedly induced in a wide variety of diseases characterized by inflammation, remodeling, and aging (17, 60–62). Recent studies have provided insights into the roles that CHI3L1 plays in these settings by demonstrating that CHI3L1 is a critical regulator of cell death, inflammation, dendritic cell accumulation and activation, oxidant injury, macrophage differentiation, bacterial clearance, innate immunity, and host tolerance to infection (18, 20, 25, 36, 63, 64). They also highlighted the mechanism(s) that CHI3L1 uses in many of these settings by demonstrating that CHI3L1 binds to and signals via IL-13Rα2 (28). The ability of CHI3L1 to regulate apoptosis via IL-13Rα2 was a prominent finding in the earlier studies of CHI3L1–IL-13Rα2 interactions (28) and is reinforced in the current studies, which demonstrate that the CHI3L1/IL-13Rα2 axis is a critical regulator of the levels of basal and bleomycin-stimulated epithelial apoptosis. The present studies demonstrate that CHI3L1 also binds to and signals via CRTH2. They also demonstrate, for the first time to our knowledge, that this binding plays a critical role in CHI3L1-induced fibroproliferative repair. In accordance with the importance of M2 macrophages and fibroblast activation in fibrogenesis (27), these studies also demonstrate that CRTH2 plays a key role in CHI3L1-induced M2 macrophage differentiation and allow for the speculation that CRTH2 also plays a role in fibroblast proliferation and activation and other fibroproliferative events. Overall, these findings demonstrate that there is more than one CHI3L1 receptor and that they differ in the mechanisms they use to traffic to the cell membrane and the effector responses they activate. Importantly, they also demonstrate that the lung pathology in HPS is mediated, at least in part, by the differential regulation of these receptors and their receptor responses. When viewed in combination, these studies demonstrate that dysregulation of CHI3L1, abnormal IL-13Rα2 trafficking, and normal CRTH2 trafficking are fundamental events in BLOC-3 HPS lung disease and allow for the conceptualization presented in Figure 8D. These findings are similar in many ways to the well-documented relationship between glucose, hepatic lipid responses, and insulin resistance in diabetes. In these patients, whole-body insulin resistance results in hyperglycemia despite increased levels of circulating insulin, with the increased levels of insulin driving hepatic lipogenesis and the development of fatty liver (65, 66). Overall, these studies suggest that interventions that increase IL-13Rα2 membrane localization and block CRTH2 function, alone or in combination, could be used to treat BLOC-3 HPS patients. Additional investigation will be required to test this speculation.

Bleomycin is well known to induce acute injury and later fibroproliferative responses in the lung. One of the interesting findings in these and previous (27) studies was that the levels of CHI3L1 decreased during the former and increased remarkably during the latter. On superficial analysis it is hard to understand how these divergent responses both contribute to the generation of pulmonary fibrosis. Since WT mice and *pale ear* mice manifest similar biphasic responses, it is also difficult to understand how this biphasic response contributes to the exaggerated responses in *pale ear* mice. However, the answers to these questions bring forth a number of important points. First, studies from our laboratory have demonstrated that oxidant injury is a powerful inhibitor of CHI3L1 and that if oxidant inhibition of CHI3L1 is prevented, oxidant injury and lung epithelial cell apoptosis are abrogated (36). Similar results were found in experiments with bleomycin (27). This suggests that a decrease in CHI3L1 appears to be a prerequisite for agents such as hyperoxia or bleomycin to induce the acute and severe tissue injury and alveolar epithelial cell death responses that they generate. Since it is well known that injury is a prerequisite for the development of tissue fibrosis (30), one can see how this decrease in CHI3L1 is required to allow fibrosis to be generated. As regards the exaggerated injury and fibrotic responses in *pale ear* mice, there are a number of important differences between the responses in these mice that need to be highlighted. First, in the *pale ear* mice there are exaggerated levels of CHI3L1 at baseline and at days 7 to 14, when these levels exceed those in WT mice. Interestingly, although CHI3L1 was a powerful inhibitor of apoptosis in WT mice and the levels of CHI3L1 were increase in *pale ear* mice, CHI3L1 did not inhibit apoptosis in the *Hps1* mutant animals. This apparent lack of CHI3L1 effect in the *pale ear* mice appears

to be due, at least in part, to alterations in IL-13Rα2 biology. The most important alteration appears to be the impressive defect in trafficking and membrane localization that can be seen at baseline and after bleomycin administration. However, we cannot rule out a modest contribution by the decrease in bleomycin-induced gene expression that is seen during the fibroproliferative repair phase in *pale ear* versus WT lungs. From these observations it is clear that the ability of bleomycin to decrease CHI3L1 is a prerequisite for the development of pulmonary fibrosis in WT and *pale ear* mice. It is also clear that the exaggerated levels of CHI3L1 and abnormal trafficking and possibly gene expression of IL-13Rα2 play critical roles in the exaggerated apoptotic/injury and fibrotic responses that are seen. Additional investigation will be required to identify the mechanisms that drive this biphasic response.

Our studies demonstrate that the levels of circulating CHI3L1 are increased in BLOC-3 HPS patients, where they associate with disease severity. They also demonstrate that the levels that are seen are higher than in patients with HPS mutations that are not associated with lung disease. At present, we do not know whether this increase is due solely to the ongoing injury response caused the abnormal trafficking of IL-13Rα2. Alternatively, it could represent a feedback mechanism that is attempting to control tissue injury. Nonetheless, these observations suggest that the levels of circulating CHI3L1 might be a clinically useful biomarker that predicts the development or rate of progression of lung disease in BLOC-3 HPS patients. It is important to point out, however, that we do not have longitudinal studies that address these possibilities. We are lacking extensive demographic information, and we also cannot rule out a confounder effect based on the number of patients of Puerto Rican ancestry in our patient cohort. Thus, additional investigation will be required to determine whether the levels of circulating CHI3L1 are truly a useful predictor of disease progression in HPS.

In summary, the present studies demonstrate that BLOC-3 HPS is associated with higher levels of CHI3L1 and suggest that CHI3L1 is likely produced as a protective response based on its ability to simultaneously decrease epithelial cell apoptosis and stimulate fibroproliferative repair in normal individuals. However, in BLOC-3 HPS, the ability of CHI3L1 to inhibit epithelial cell apoptosis is impaired due, at least in part, to faulty trafficking and insufficient membrane expression of the CHI3L1 receptor IL-13Rα2. On the other hand, the sustained and enhanced production of CHI3L1 interacts with CRTH2, which traffics normally, and causes an exaggerated fibroproliferative repair response and fibrotic excess in BLOC-3 HPS patients. Additional investigations of the roles of CHI3L1 and its receptors in HPS and related diseases are warranted.

Methods

Patient characteristics. One hundred and forty-seven samples were obtained from molecularly confirmed HPS patients ≥18 years of age with or without known lung disease (based on high-resolution CT [HRCT] evaluation) that were enrolled in a clinical protocol approved by the NHGRI Institutional Review Board. Of the 147 patients, 129 had BLOC-3–related HPS (125 HPS-1 and 4 HPS-4) and 18 had BLOC-2–related disease (12 HPS-3, 4 HPS-5, and 2 HPS-6). The mean age of BLOC-3–related patients was 37.7 ± 0.9 years, while the mean age of the BLOC-3–unrelated patients was 36.3 ± 2.9 (P = 0.46). All HPS patients underwent pulmonary function tests (PFTs). The mean FVC in the BLOC-3–related subjects was 76.7 ± 1.0 versus 94.0 ± 2.6 (P = 0.0002). The mean DLCO in the BLOC-3–related subjects was 72.0 ± 2.0 versus 103.6 ± 3.5 (P < 0.0001). The normal controls and IPF patients were recruited from the Translational Lung Research Program at the Yale School of Medicine as previously described (27).

ELISA. Human CHI3L1 was assayed using a commercially available ELISA kit (Quidel) as previously described (63). CHI3L1 levels in mouse BAL samples were quantified using coating and detection antibodies from MedImmune. TGF-β1 levels in mouse BAL samples were quantified using an ELISA kit (R&D Systems) following the manufacturer's instructions.

Knockout and Tg mice. *Pale ear* mice were obtained from The Jackson Laboratory (*Hps1*^{ep}). *Chi3l1 (Brp39)* knockout mice (*Chi3l1*$^{-/-}$) and *Cc10*-driven, lung-specific, inducible *CHI3L1 (YKL-40)* Tg mice (*CHI3L1* Tg) were previously generated in our laboratory (20), and Tg(*Cc10-Il13*) mice (referred to as *Il13* Tg mice) were previously described (67). *CHI3L1* Tg mice or their WT littermate controls (transgene negative) were given doxycycline (1 g/l) in their drinking water for up to 2 weeks. All mice were congenic on a C57BL/6 background and were genotyped as previously described.

Bleomycin administration. Sex-matched, 8-week-old WT, *pale ear*, *Chi3l1*$^{-/-}$, and *CHI3L1* Tg mice (≥4 mice/group/experiment, repeated at least three times) were exposed to a single bleomycin injection (1.25 U/kg; Teva Parenteral Medicines) via intratracheal administration. Mice were sacrificed and evaluated on day 7 and day 14 to examine apoptosis and fibrosis, respectively.

mRNA analysis. Total cellular RNA was obtained using TRIzol reagent (Invitrogen), according to the manufacturer's instructions. mRNA was measured using quantitative real-time RT-PCR (qRT-PCR) as described previously (20, 21). The primer sequences for extracellular matrix genes were obtained from PrimerBank (pga.mgh.harvard.edu/primerbank/) or were the same as previously used (20, 68, 69).

Histologic analysis. Mouse lungs were removed en bloc, inflated to 25 cm pressure with PBS containing 0.5% low-melting-point agarose gel, fixed, embedded in paraffin, sectioned, and stained. H&E and Mallory's trichrome stainings were performed in the Research Histology Laboratory of the Department of Pathology at the Yale University School of Medicine. BAL and lung inflammation were assessed as described previously (20).

Quantification of lung collagen. Animals were anesthetized, median sternotomy was performed, and right heart perfusion was completed with calcium- and magnesium-free PBS. The heart and lungs were then removed. The right lung was frozen in liquid nitrogen and stored at –80°C until used. Collagen content was determined by quantifying total soluble collagen using the Sircol Collagen Assay kit (Biocolor, Accurate Chemical & Scientific Corp.) according to the manufacturer's instructions.

TUNEL analysis. End labeling of exposed 3′-OH ends of DNA fragments in paraffin-embedded tissue was undertaken with the TUNEL in situ cell death detection kit AP (Roche Diagnostics). SPC costaining was performed using a goat anti-mouse SPC primary antibody (Santa Cruz Biotechnology Inc., #sc-7706) and Alexa Fluor 594 secondary antibody (Life Technologies, #A-11058). After staining, 8 to 10 random pictures were obtained from each lung, and a minimum of 300 cells were visually evaluated in each section. The labeled cells were expressed as a percentage of total nuclei.

Immunofluorescence staining and immunohistochemistry. To localize the expression of IL-13Rα2 and CRTH2, double-label immunofluorescence staining was undertaken using paraffin-embedded lungs from WT and *pale ear* mice. Monoclonal anti–IL-13Rα2 (R&D Systems, #MAB539), anti-CRTH2 (Santa Cruz Biotechnology Inc., #sc-23093), and antibodies against pan-cadherin (Abcam, #ab16505) and EEA1 (Abcam #ab2900 and Cell Signaling Technology #3288) were used in these evaluations. To localize the expression of IL-13Rα2 in humans, lung biopsies from normal, IPF (27), and HPS-1 patients were obtained, and immunofluorescence staining was undertaken. Polyclonal anti–IL-13Rα2 antibody (Millipore, #06-1091) was used in these evaluations. Immunohistochemical analysis of HPS lungs was performed as previously described (27).

Live cell confocal imaging. WT and *pale ear* mouse lungs were digested with collagenase and DNase I. The resulting suspension was filtered through Falcon cell strainers, and the cells were negatively selected with anti-CD16/CD32 antibodies (eBioscience, #14-0161). Cells were maintained in BEGM + 5% charcoal-stripped FBS and 10 ng/ml KGF. Mouse IL-13Rα2–tGFP fusion protein plasmid was constructed (Origene) and expressed in WT and *pale ear* primary type II cells (500 ng/well). Cells were stimulated with 100 μg/ml bleomycin and imaged every 5 minutes. DRAQ5 was used to stain the nuclei (Thermo-Fisher).

Cell culture. Primary type II cells were pretreated with 500 ng/ml recombinant CHI3L1, transfected with IL-13Rα2 construct (3 μg/well), and stimulated with 100 μg/ml bleomycin. A549 cells were obtained from ATCC and maintained in DMEM + 2 mM glutamine + 10 % FBS. HPS1, HPS4, Rab32, and/or Rab38 siRNA were cotransfected with IL-13Rα2 construct (3 μg/well) and stimulated with 100 μg/ml bleomycin. Cells were cytospun onto slides. Immunofluorescence and/or TUNEL staining was performed as previously described. Mouse peritoneal macrophages were obtained as previously described (28). Cells were transfected with control or CRTH2 siRNA and treated recombinant CHI3L1 (500 ng/ml) for 24 hours.

Western blot analysis. Lung and cell lysates were fractioned using a Plasma Membrane Protein Extraction Kit (Abcam), and Western blot analysis was completed with antibodies that react selectively with IL-13Rα2 (R&D Systems, #MAB539), EEA1 (Abcam, #ab2900), pan-cadherin (Abcam, #ab16505), and GAPDH (Cell Signaling Technology, #3683S) as described previously (30).

Yeast two-hybrid screening. Yeast two-hybrid screening was performed as previously described (28). Briefly, full-length murine *Chi3l1* DNA was cloned into the yeast two-hybrid BD vector at the *BamHI* and *Sal1* sites. The Matchmaker System 3 two-hybrid assay using *Saccharomyces cerevisiae* (Clontech) was used to detect interactions between CHI3L1 and other cellular proteins. *S. cerevisiae* strain AH109 (Clontech) containing the four reporter genes *ADE2*, *HIS3*, *MEL1*, and *lacZ* was cotransfected with the pGBKT7-CHI3L1 bait plasmid and the mouse lung cDNA library (Clontech) constructed into the vector pAC2 by the lithium acetate method. All positive constructs were rescreened for their ability to grow on complete dropout medium when transfected together with the CHI3L1 bait or with the empty pGBKT7 plasmid to verify potential interactions and to eliminate false positives.

Co-IP. Proteins from the lung lysate of WT mice or *Il13* Tg mice were clarified by centrifugation for 10 minutes at 4°C. CHI3L1 and CRTH2 were immunoprecipitated with anti-CHI3L1 rabbit polyclonal antibody (MedImmune) or anti-CRTH2 monoclonal antibody (Santa Cruz Biotechnology Inc.), respectively, using Catch and Release v2.0 Reversible Immunoprecipitation System (EMD Millipore). The precipitates were subjected to immunoblotting with antibodies against CRTH2 or CHI3L1, respectively.

FACS analysis. THP-1 cells (ATCC) were incubated in the presence or absence of anti-CHI3L1–biotin antibody and anti-CRTH2 IgG antibody without permeabilization. Cells were then washed and stained with streptavidin-PE and anti-IgG–APC and subjected to flow cytometric analysis.

CRTH2 inhibition. Sex-matched, 8-week-old WT, *pale ear*, and *CHI3L1* Tg mice (≥5 mice/group) were exposed to a single bleomycin injection (1.25 U/kg; Teva Parenteral Medicines) via intratracheal administration. Mice were treated with 30 mg/kg CAY10471 (Cayman Chemical) (i.p., every other day) or DMSO control from day 5 to day 14.

Statistics. Human data are presented as dot plots with median and interquartile ranges unless stated otherwise. Data distribution was assessed with the D'Agostino and Pearson omnibus test. Normally distributed data were compared using ANOVA with Bonferroni's post hoc test as appropriate. Non-normally distributed data in two groups were compared using the nonparametric two-tailed Mann-Whitney *U* test. Correlations between pulmonary function and plasma CHI3L1 concentrations were performed for those subjects on whom clinical data were available using Spearman correlations. GraphPad Prism 5.0 (GraphPad Software) and SPSS 13.0 (SPSS Inc.) were used for the analysis. Mouse data are expressed as mean ± SEM. As appropriate, groups were compared by ANOVA with Bonferroni's post hoc test; follow-up comparisons between groups were conducted using a two-tailed Student *t* test. A P value of ≤0.05 was considered significant.

Study approval. HPS patients were enrolled in a clinical protocol approved by the NHGRI Institutional Review Board. All patients gave written informed consent for protocols 95-HG-0193 and/or 04-HG-0211. Animal experiments were approved by the Institutional Animal Care and Use Committee of the Yale School of Medicine and Brown University in accordance with federal guidelines.

Acknowledgments

Funding was provided by the American Thoracic Society/Hermansky-Pudlak Syndrome Network (to Y. Zhou); HL-R01 HL093017 and U01HL108638 (to J.A. Elias); R01HL-109033 (to E.L. Herzog); R01 HL115813 (to C.G. Lee); P20 GM103652 Pilot (to Y. Zhou); and the Intramural Research Program, NHGRI, NIH.

Address correspondence to: Jack A. Elias, Frank L. Day Professor of Biology and Medicine, Dean of Medicine and Biologic Sciences, Brown University, Warren Alpert Medical School, Box G-A1, 97 Waterman Street, Providence, Rhode Island 02912, USA. Phone: 401.863.3336; E-mail: jack_elias@brown.edu.

1. Gahl WA, Huizing M. Hermansky-Pudlak syndrome. In: Pagon RA, Adam MP, Ardinger HH, eds. *GeneReviews*. Seattle, Washington, USA: University of Washington; 2012.
2. Schinella RA, Greco MA, Cobert BL, Denmark LW, Cox RP. Hermansky-Pudlak syndrome with granulomatous colitis. *Ann Intern Med*. 1980;92(1):20–23.
3. Anderson PD, Huizing M, Claassen DA, White J, Gahl WA. Hermansky-Pudlak syndrome type 4 (HPS-4): clinical and molecular characteristics. *Hum Genet*. 2003;113(1):10–17.
4. Gahl WA, et al. Genetic defects and clinical characteristics of patients with a form of oculocutaneous albinism (Hermansky-Pudlak syndrome).

N Engl J Med. 1998;338(18):1258–1264.
5. Hermansky F, Pudlak P. Albinism associated with hemorrhagic diathesis and unusual pigmented reticular cells in the bone marrow: report of two cases with histochemical studies. *Blood*. 1959;14(2):162–169.
6. Tsilou ET, et al. Milder ocular findings in Hermansky-Pudlak syndrome type 3 compared with Hermansky-Pudlak syndrome type 1. *Ophthalmology*. 2004;111(8):1599–1603.
7. Parker MS, et al. The Hermansky-Pudlak syndrome. *Ann Diagn Pathol*. 1997;1(2):99–103.
8. Mahadeo R, Markowitz J, Fisher S, Daum F. Hermansky-Pudlak syndrome with granulomatous colitis in children. *J Pediatr*. 1991;118(6):904–906.
9. Li W, Rusiniak ME, Chintala S, Gautam R, Novak EK, Swank RT. Murine Hermansky-Pudlak syndrome genes: regulators of lysosome-related organelles. *Bioessays*. 2004;26(6):616–628.
10. Brantly M, Avila NA, Shotelersuk V, Lucero C, Huizing M, Gahl WA. Pulmonary function and high-resolution CT findings in patients with an inherited form of pulmonary fibrosis, Hermansky-Pudlak syndrome, due to mutations in HPS-1. *Chest*. 2000;117(1):129–136.
11. Chiang PW, Oiso N, Gautam R, Suzuki T, Swank RT, Spritz RA. The Hermansky-Pudlak syndrome 1 (HPS1) and HPS4 proteins are components of two complexes, BLOC-3 and BLOC-4, involved in the biogenesis of lysosome-related organelles. *J Biol Chem*. 2003;278(22):20332–20337.
12. Carmona-Rivera C, Simeonov DR, Cardillo ND, Gahl WA, Cadilla CL. A divalent interaction between HPS1 and HPS4 is required for the formation of the biogenesis of lysosome-related organelle complex-3 (BLOC-3). *Biochim Biophys Acta*. 2013;1833(3):468–478.
13. Pierson DM, et al. Pulmonary fibrosis in Hermansky-Pudlak syndrome. a case report and review. *Respiration*. 2006;73(3):382–395.
14. Young LR, Pasula R, Gulleman PM, Deutsch GH, McCormack FX. Susceptibility of Hermansky-Pudlak mice to bleomycin-induced type II cell apoptosis and fibrosis. *Am J Respir Cell Mol Biol*. 2007;37(1):67–74.
15. Lee CG, et al. Role of chitin and chitinase/chitinase-like proteins in inflammation, tissue remodeling, and injury. *Annu Rev Physiol*. 2011;73:479–501.
16. Aerts JM, et al. Biomarkers for lysosomal storage disorders: identification and application as exemplified by chitotriosidase in Gaucher disease. *Acta Paediatr Suppl*. 2008;97(457):7–14.
17. Funkhouser JD, Aronson NN Jr. Chitinase family GH18: evolutionary insights from the genomic history of a diverse protein family. *BMC Evol Biol*. 2007;7:96.
18. Dela Cruz CS, et al. Chitinase 3-like-1 promotes Streptococcus pneumoniae killing and augments host tolerance to lung antibacterial responses. *Cell Host Microbe*. 2012;12(1):34–46.
19. Lee CG, Elias JA. Role of breast regression protein-39/YKL-40 in asthma and allergic responses. *Allergy Asthma Immunol Res*. 2010;2(1):20–27.
20. Lee CG, et al. Role of breast regression protein 39 (BRP-39)/chitinase 3-like-1 in Th2 and IL-13-induced tissue responses and apoptosis. *J Exp Med*. 2009;206(5):1149–1166.
21. Sohn MH, et al. The chitinase-like proteins breast regression protein-39 and YKL-40 regulate hyperoxia-induced acute lung injury. *Am J Respir Crit Care Med*. 2010;182(7):918–928.
22. Areshkov PO, Avdieiev SS, Balynska OV, Leroith D, Kavsan VM. Two closely related human members of chitinase-like family, CHI3L1 and CHI3L2, activate ERK1/2 in 293 and U373 cells but have the different influence on cell proliferation. *Int J Biol Sci*. 2012;8(1):39–48.
23. Chen C-C, Llado V, Eurich K, Tran HT, Mizoguchi E. Carbohydrate-binding motif in chitinase 3-like 1 (CH13L1/YKL-40) specifically activates Akt signaling pathway in colonic epithelial cells. *Clin Immunol*. 2011;140(3):268–275.
24. Kim MN, et al. Involvement of the MAPK and PI3K pathways in chitinase 3-like 1-regulated hyperoxia-induced airway epithelial cell death. *Biochem Biophys Res Commun*. 2012;421(4):790–796.
25. Matsuura H, et al. Role of breast regression protein-39 in the pathogenesis of cigarette smoke-induced inflammation and emphysema. *Am J Respir Cell Mol Biol*. 2011;44(6):777–786.
26. Coffman FD. Chitinase 3-Like-1 (CHI3L1): a putative disease marker at the interface of proteomics and glycomics. *Crit Rev Clin Lab Sci*. 2008;45(6):531–562.
27. Zhou Y, et al. Chitinase 3-like 1 suppresses injury and promotes fibroproliferative responses in Mammalian lung fibrosis. *Sci Transl Med*. 2014;6(240):240ra76.
28. He CH, et al. Chitinase 3-like 1 regulates cellular and tissue responses via IL-13 receptor α2. *Cell Rep*. 2013;4(4):830–841.
29. Young LR, Borchers MT, Allen HL, Gibbons RS, McCormack FX. Lung-restricted macrophage activation in the pearl mouse model of Hermansky-Pudlak syndrome. *J Immunol*. 2006;176(7):4361–4368.
30. Lee CG, et al. Early growth response gene 1-mediated apoptosis is essential for transforming growth factor beta1-induced pulmonary fibrosis. *J Exp Med*. 2004;200(3):377–389.
31. Gerondopoulos A, Langemeyer L, Liang JR, Linford A, Barr FA. BLOC-3 mutated in Hermansky-Pudlak syndrome is a Rab32/38 guanine nucleotide exchange factor. *Curr Biol*. 2012;22(22):2135–2139.
32. Murray LA, et al. Targeting interleukin-13 with tralokinumab attenuates lung fibrosis and epithelial damage in a humanized SCID idiopathic pulmonary fibrosis model. *Am J Respir Cell Mol Biol*. 2014;50(5):985–994.
33. Konishi K, et al. Gene expression profiles of acute exacerbations of idiopathic pulmonary fibrosis. *Am J Respir Crit Care Med*. 2009;180(2):167–175.
34. Young LR, et al. The alveolar epithelium determines susceptibility to lung fibrosis in Hermansky-Pudlak syndrome. *Am J Respir Crit Care Med*. 2012;186(10):1014–1024.
35. Avila NA, Brantly M, Premkumar A, Huizing M, Dwyer A, Gahl WA. Hermansky-Pudlak syndrome: radiography and CT of the chest compared with pulmonary function tests and genetic studies. *AJR Am J Roentgenol*. 2002;179(4):887–892.
36. Sohn MH, et al. The chitinase-like proteins breast regression protein-39 and YKL-40 regulate hyperoxia-induced acute lung injury. *Am J Respir Crit Care Med*. 2009;182(7):918–928.
37. Swank RT, Novak EK, McGarry MP, Rusiniak ME, Feng L. Mouse models of Hermansky Pudlak syndrome: a review. *Pigment Cell Res*. 1998;11(2):60–80.
38. Feng L, Rigatti BW, Novak EK, Gorin MB, Swank RT. Genomic structure of the mouse Ap3b1 gene in normal and pearl mice. *Genomics*. 2000;69(3):370–379.
39. Mahavadi P, et al. Epithelial stress and apoptosis underlie Hermansky-Pudlak syndrome-associated interstitial pneumonia. *Am J Respir Crit Care Med*. 2010;182(2):207–219.
40. Yoshioka Y, et al. Inflammatory response and cathepsins in silica-exposed Hermansky-Pudlak syndrome model pale ear mice. *Pathol Int*. 2004;54(5):322–331.
41. Rouhani FN, et al. Alveolar macrophage dysregulation in Hermansky-Pudlak syndrome type 1. *Am J Respir Crit Care Med*. 2009;180(11):1114–1121.
42. Atochina-Vasserman EN, et al. Early alveolar epithelial dysfunction promotes lung inflammation in a mouse model of Hermansky-Pudlak syndrome. *Am J Respir Crit Care Med*. 2011;184(4):449–458.
43. Lupardus PJ, Birnbaum ME, Garcia KC. Molecular basis for shared cytokine recognition revealed in the structure of an unusually high affinity complex between IL-13 and IL-13Rα2. *Structure*. 2010;18(3):332–342.
44. Strober W, Kitani A, Fichtner-Feigl S, Fuss IJ. The signaling function of the IL-13Rα2 receptor in the development of gastrointestinal fibrosis and cancer surveillance. *Curr Mol Med*. 2009;9(6):740–750.
45. Konstantinidis AK, et al. Cellular localizataion of interleukin 13 receptor α2 in human primary bronchial epithelial cells and fibroblasts. *J Investig Allergol Clin Immunol*. 2008;18(3):174–180.
46. Daines MO, et al. Level of expression of IL-13Ralpha2 impacts receptor distribution and IL-13 signaling. *J Immunol*. 2006;176(12):7495–7501.
47. Fichtner-Feigl S, et al. Induction of IL-13 triggers TGF-beta1-dependent tissue fibrosis in chronic 2,4,6-trinitrobenzene sulfonic acid colitis. *J Immunol*. 2007;178(9):5859–5870.
48. Fichtner-Feigl S, Strober S, Kawakami K, Puri RK, Kitani A. IL-13 signaling through the IL-13α(2) receptor is involved in induction of TGF-β(1) production and fibrosis. *Nat Med*. 2006;12(1):99–106.
49. Fichtner-Feigl S, Strober W, Geissler EK, Schlitt H-J. Cytokines mediating the induction of chronic colitis and colitis-associated fibrosis. *Mucosal Immunol*. 2008;1(suppl 1):S24–S27.
50. Fichtner-Feigl S, et al. Restoration of tumor immunosurveillance via targeting of interleukin-13 receptor-α2. *Cancer Res*. 2008;68(9):3467–3475.
51. Yang JS, Allahverdian S, Singhera GK, MacRedmond RE, Dorscheid DR. IL-13Rα2/AP-1 complex signalling mediates airway epithelial repair without effects on remodeling pathways. *Allergy Asthma Clin Immunol*. 2010;6(suppl 3):P27.
52. Yang JSY, Wadsworth SJ, Singhera GK, Dorscheid D. The regulation of IL-13rα1 and IL-13rα2 expression and distribution in airway epithelial repair. *Am J Respir Crit Care Med*. 2011;183(3):174–180.
53. Daines MO, Hershey GK. A novel mechanism

by which interferon-γ can regulate interleukin (IL)-13 responses. Evidence for intracellular stores of IL-13 receptor α-2 and their rapid mobilization by interferon-γ. *J Biol Chem*. 2002;277(12):10387–10393.
54. Tabata Y, Chen W, Warrier MR, Gibson AM, Daines MO, Hershey GK. Allergy-driven alternative splicing of IL-13 receptor α2 yields distinct membrane and soluble forms. *J Immunol*. 2006;177(11):7905–7912.
55. Chiaramonte MG, et al. Regulation and function of the interleukin 13 receptor α2 during a T helper cell type 2-dominant immune response. *J Exp Med*. 2003;197(6):687–701.
56. Wilson MS, et al. IL-13Rα2 and IL-10 coordinately suppress airway inflammation, airway-hyperreactivity, and fibrosis in mice. *J Clin Invest*. 2007;117(10):2941–2951.
57. Wasmeier C, Romao M, Plowright L, Bennett DC, Raposo G, Seabra MC. Rab38 and Rab32 control post-Golgi trafficking of melanogenic enzymes. *J Cell Biol*. 2006;175(2):271–281.
58. Mackinnon AC, et al. Regulation of transforming growth factor-β1-driven lung fibrosis by galectin-3. *Am J Respir Crit Care Med*. 2012;185(5):537–546.
59. Cullinane AR, et al. Dysregulation of galectin-3. Implications for Hermansky-Pudlak syndrome pulmonary fibrosis. *Am J Respir Cell Mol Biol*. 2014;50(3):605–613.
60. Bussink AP, Speijer D, Aerts JM, Boot RG. Evolution of mammalian chitinase(-like) members of family 18 glycosyl hydrolases. *Genetics*. 2007;177(2):959–970.
61. Kzhyshkowska J, Gratchev A, Goerdt S. Human chitinases and chitinase-like proteins as indicators for inflammation and cancer. *Biomark Insights*. 2007;2:128–146.
62. Bojesen SE, Johansen JS, Nordestgaard BG. Plasma YKL-40 levels in healthy subjects from the general population. *Clin Chim Acta*. 2011; 412(9–10):709–712.
63. Chupp GL, et al. A chitinase-like protein in the lung and circulation of patients with severe asthma. *N Engl J Med*. 2007;357(20):2016–2027.
64. Lee CG, et al. Role of chitin and chitinase/chitinase-like proteins in inflammation, tissue remodeling, and injury. *Annu Rev Physiol*. 2011;73:479–501.
65. DeFronzo RA, Gunnarsson R, Bjorkman O, Olsson M, Wahren J. Effects of insulin on peripheral and splanchnic glucose metabolism in noninsulin-dependent (type II) diabetes mellitus. *J Clin Invest*. 1985;76(1):149–155.
66. Marchesini G, et al. Association of nonalcoholic fatty liver disease with insulin resistance. *Am J Med*. 1999;107(5):450–455.
67. Zhu Z, et al. Pulmonary expression of interleukin-13 causes inflammation, mucus hypersecretion, subepithelial fibrosis, physiologic abnormalities, and eotaxin production. *J Clin Invest*. 1999;103(6):779–788.
68. Zhou Y, et al. Amphiregulin, an epidermal growth factor receptor ligand, plays an essential role in the pathogenesis of transforming growth factor-β-induced pulmonary fibrosis. *J Biol Chem*. 2012;287(50):41991–42000.
69. Kang HR, Lee CG, Homer RJ, Elias JA. Semaphorin 7A plays a critical role in TGF-β1-induced pulmonary fibrosis. *J Exp Med*. 2007;204(5):1083–1093.